The Astrophysical Journal, 773:73 (11pp), 2013 August 10 doi:10.1088/0004-637X/773/1/73

THE SEEDS DIRECT IMAGING SURVEY FOR PLANETS AND SCATTERED DUST EMISSION IN DEBRIS DISK SYSTEMS

Markus Janson[1,28], Timothy D. Brandt[1], Amaya Moro-Martín[2], Tomonori Usuda[3], Christian Thalmann[4], Joseph C. Carson[5,6], Miwa Goto[7], Thayne Currie[8], M. W. McElwain[9], Yoichi Itoh[10], Misato Fukagawa[11], Justin Crepp[12], Masayuki Kuzuhara[13], Jun Hashimoto[13], Tomoyuki Kudo[3], Nobuhiko Kusakabe[13], Lyu Abe[14], Wolfgang Brandner[6], Sebastian Egner[3], Markus Feldt[6], Carol A. Grady[15], Olivier Guyon[3], Yutaka Hayano[3], Masahiro Hayashi[3], Saeko Hayashi[3], Thomas Henning[6], Klaus W. Hodapp[16], Miki Ishii[3], Masanori Iye[13], Ryo Kandori[13], Gillian R. Knapp[1], Jungmi Kwon[17], Taro Matsuo[18], Shoken Miyama[19], Jun-Ichi Morino[13], Tetsuro Nishimura[3], Tae-Soo Pyo[3], Eugene Serabyn[20], Takuya Suenaga[17], Hiroshi Suto[13], Ryuji Suzuki[21], Yasuhiro Takahashi[22], Michihiro Takami[23], Naruhisa Takato[3], Hiroshi Terada[3], Daego Tomono[3], Edwin L. Turner[1,24], Makoto Watanabe[25], John Wisniewski[26], Toru Yamada[27], Hideki Takami[3], and Motohide Tamura[13]

[1] Department of Astrophysical Sciences, Princeton University, NJ 08544, USA; janson@astro.princeton.edu
[2] Department of Astrophysics, CAB (INTA-CSIC), Instituto Nacional de Técnica Aerospacial, Torrejónde Ardoz, E-28850 Madrid, Spain
[3] Subaru Telescope, 650 North Aohoku Place, Hilo, HI 96720, USA
[4] Astronomical Institute "Anton Pannekoek," University of Amsterdam, Science Park 904, 1098-XH Amsterdam, The Netherlands
[5] Department of Physics and Astronomy, College of Charleston, 58 Coming Street, Charleston, SC 29424, USA
[6] Max Planck Institute for Astronomy, Königstuhl 17, D-69117 Heidelberg, Germany
[7] Universitäts-Sternwarte München, Ludwig-Maximilians-Universität, Scheinerstr. 1, D-81679 Munich, Germany
[8] Department of Astronomy and Astrophysics, University of Toronto, 50 St. George Street, M5S 3H4 Toronto, ON, Canada
[9] Exoplanets and Stellar Astrophysics Laboratory, Code 667, Goddard Space Flight Center, Greenbelt, MD 2071, USA
[10] Nishi-Harima Astronomical Observatory, Center for Astronomy, University of Hyogo, 407-2 Nishigaichi, Sayo, Hyogo 679-5313, Japan
[11] Department of Earth and Space Science, Graduate School of Science, Osaka University, 1-1 Machikaneyama, Toyonaka, Osaka 560-0043, Japan
[12] Department of Physics, University of Notre Dame, 225 Nieuwland Science Hall, Notre Dame, IN 46556, USA
[13] National Astronomical Observatory of Japan, 2-21-1 Osawa, Mitaka, Tokyo 181-8588, Japan
[14] Laboratoire Lagrange, UMR7239, University of Nice-Sophia Antipolis, CNRS, Observatoire de la Cote d'Azur, F-06300 Nice, France
[15] Eureka Scientific, 2452 Delmer, Suite 100, Oakland, CA 96002, USA
[16] Institute for Astronomy, University of Hawai'i, 640 North A'ohoku Place, Hilo, HI 96720, USA
[17] Department of Astronomical Science, Graduate University for Advanced Studies (Sokendai), Tokyo 181-8588, Japan
[18] Department of Astronomy, Kyoto University, Kitsahirakawa-Oiwake-cho, Sakyo-ku, Kyoto 606-8502, Japan
[19] Office of the President, Hiroshima University, 1-3-2 Kagamiyama, Hagashi-Hiroshima 739-8511, Japan
[20] Jet Propulsion Laboratory, California Institute of Technology, Pasadena, CA 91109, USA
[21] TMT Observatory Corporation, 1111 South Arroyo Parkway, Pasadena, CA 91105, USA
[22] Department of Astronomy, The University of Tokyo, Hongo 7-3-1, Bunkyo-ku, Tokyo 113-0033, Japan
[23] Institute of Astronomy and Astrophysics, Academia Sinica, P.O. Box 23-141, Taipei 106, Taiwan
[24] Kavli Institute for the Physics and Mathematics of the Universe, The University of Tokyo, Kashiwa 277-8568, Japan
[25] Department of Cosmosciences, Hokkaido University, Sapporo 060-0810, Japan
[26] H.L. Dodge Department of Physics and Astronomy, University of Oklahoma, 440 West Brooks Street, Norman, OK 73019, USA
[27] Astronomical Institute, Tohoku University, Aoba, Sendai 980-8578, Japan
Received 2013 March 6; accepted 2013 June 1; published 2013 July 26

ABSTRACT

Debris disks around young main-sequence stars often have gaps and cavities which for a long time have been interpreted as possibly being caused by planets. In recent years, several giant planet discoveries have been made in systems hosting disks of precisely this nature, further implying that interactions with planets could be a common cause of such disk structures. As part of the SEEDS high-contrast imaging survey, we are surveying a population of debris-disk-hosting stars with gaps and cavities implied by their spectral energy distributions, in order to attempt to spatially resolve the disk as well as to detect any planets that may be responsible for the disk structure. Here, we report on intermediate results from this survey. Five debris disks have been spatially resolved, and a number of faint point sources have been discovered, most of which have been tested for common proper motion, which in each case has excluded physical companionship with the target stars. From the detection limits of the 50 targets that have been observed, we find that β Pic b-like planets ($\sim$10 $M_{\rm jup}$ planets around G–A-type stars) near the gap edges are less frequent than 15%–30%, implying that if giant planets are the dominant cause of these wide (27 AU on average) gaps, they are generally less massive than β Pic b.

Key words: circumstellar matter – planetary systems – stars: early-type

Online-only material: color figures

1. INTRODUCTION

The close circumstellar environment around mature (post-T Tauri and Herbig Ae/Be) stars has traditionally been difficult to study directly, due to the strong flux from the star itself, which drowns out the light of its physical surroundings over a wide range of wavelengths. However, developments in high-contrast and high-resolution instruments and techniques have made this environment increasingly accessible to detailed study in recent years. Several surveys have been performed (e.g., Kasper et al. 2007; Lafrenière et al. 2007a; Rameau et al. 2013) and a number

[28] Hubble fellow.

of extrasolar planets have been imaged (e.g., Marois et al. 2010; Lagrange et al. 2010; Carson et al. 2013), and while the most extreme debris disk systems have been possible to image for some time (e.g., Smith et al. 1984), the sample of spatially resolved disks is presently growing rapidly, both in thermal (e.g., Greaves et al. 2005; Wilner et al. 2011; Acke et al. 2012) and scattered radiation (e.g., Krist et al. 2005; Kalas et al. 2005; Buenzli et al. 2010). Nonetheless, most planets and disks are still discovered only indirectly, through stellar radial velocity or transits in the case of planets (e.g., Mayor & Queloz 1995; Borucki et al. 2011) and through infrared excess in the case of disks (e.g., Beichman et al. 2006; Su et al. 2006).

The Strategic Exploration of Exoplanets and Disks with Subaru (SEEDS; Tamura 2009) is a large-scale survey using adaptive optics (AO) assisted high-contrast imaging for studying planets and disks, from primordial and transitional systems (e.g., Kusakabe et al. 2012; Muto et al. 2012; Grady et al. 2013) to mature systems. A sub-survey of this larger effort concerns the study of debris disk systems. This study has several purposes, including: (1) searching for direct light from debris disks, in the sense of acquiring spatially resolved images of disks that have previously only been identified from infrared excess, (2) searching for planets in systems with known debris disks, and (3) studying interactions and correlations between planets and debris disks. Interestingly, many of the recently imaged planets coincide with debris disks (Marois et al. 2008, 2010; Lagrange et al. 2009). Many disks also have morphological indications of the presence of dynamical influence from planets in the system (e.g., Hines et al. 2007; Buenzli et al. 2010; Thalmann et al. 2011; Currie et al. 2012b; Quanz 2013), such as eccentric gaps with sharp inner boundaries or apparently resonant dust concentrations (e.g., Quillen & Thorndike 2002; Quillen 2006), although alternative mechanisms have been suggested (e.g., Jalali & Tremaine 2012; Lyra & Kuchner 2012). Thus, stars hosting debris disks are promising targets for imaging of massive exoplanets.

In previous publications, we have presented two results from the debris disk survey, in the form of spatially resolved disks around HR 4796 A (Thalmann et al. 2011) and HIP 79977 (Thalmann et al. 2013). Here, we will summarize the results from the rest of the survey so far, including images of spatially resolved disks and detection limits for planets which are interpreted in the context of the disk architecture in the system, and which form part of the basis for a statistical study that is presently in progress (T. D. Brandt et al., in preparation). In the following, we first describe the target selection in Section 2 and the observations and data reduction in Section 3, followed by a presentation of the results in Section 4. We discuss and summarize our results in Section 5.

2. TARGET SELECTION

A master list of targets was compiled from a wide range of literature sources identifying debris disk host stars based on infrared excess as measured by telescopes such as *IRAS* and *Spitzer* (e.g., Rieke et al. 2005; Rhee et al. 2007; Trilling et al. 2008; Plavchan et al. 2009). Targets for specific SEEDS runs were then selected continuously from this list, prioritized on the basis of disk properties (fractional luminosity and predicted angular separation) and possible planet properties (ease of detection, based on proximity and youth, as well as stellar mass assuming a constant typical planet–star mass ratio). Special emphasis was placed on cold disks, characterized by the presence of dust at large physical separations but indications of gaps or cavities at smaller separations. Such gaps could be caused by planets (see, e.g., Apai et al. 2008 and references therein.), which could in turn be observable in high-contrast images. A few warm disks however were also observed—these could have planets at larger separations, and the disk in such systems should be highly luminous at small separations, where HiCIAO performs the most competitively. Some high-profile planet-search targets were purposefully omitted—these are cases where specialized deep observations have been performed in dedicated studies, upon which it would be difficult or impossible to improve in a general survey with a 1 hr observation in the *H* band. In particular, this is true for the targets ϵ Eri and Vega (Janson et al. 2008; Heinze et al. 2008). The special case of Fomalhaut (e.g., Kalas et al. 2008; Janson et al. 2012; Currie et al. 2012a; Galicher et al. 2013; Kenworthy et al. 2013) was also omitted for this reason. Histograms for the spectral type, distance, and age of the targets are shown in Figure 1.

3. OBSERVATIONS AND DATA REDUCTION

The observations were carried out as part of the SEEDS program at the Subaru telescope, using the HiCIAO camera (Tamura et al. 2006; Hodapp et al. 2008) with the AO188 AO system (Hayano et al. 2008). The bulk of observations were taken throughout 2011 and 2012, with some observations also taken in 2009 and 2010 (see Table 1). No mask was used, but the detector was instead allowed to saturate at the point spread function (PSF) core, typically out to a radius of 0.″3. All observations made use of the angular differential imaging (ADI) technique (Marois et al. 2006) with the pupil fixed on the detector, and were performed using the *H*-band filter, with a central wavelength of 1.65 μm and a bandwidth of 0.29 μm. In most cases, the instrument was set to direct imaging, but in a few cases, the polarimetric differential imaging (PDI) mode was used, in which the beam is split into two orthogonal polarization states using a Wollaston prism, with each corresponding image mapped onto one half of the detector. In those cases, the results presented here are based on separate reductions of each polarization state, which we then average together. We do not include any PDI reductions in this study. The typical telescope time spent on a target was $\sim$1 hr including overheads.

The ADI reductions were uniformly performed using the ACORNS-ADI pipeline (Brandt et al. 2013), with the same procedure as given in the ACORNS paper. As a brief summary, the data were destriped,[29] flat fielded, and corrected for field distortion. Relative centroiding was done using PSF fitting on non-saturated parts of the PSF, and absolute centering was based on visual inspection with a $\sim$0.5 pixel precision. PSF subtraction was performed with a Locally Optimized Combination of Images (LOCI) based scheme (Lafrenière et al. 2007b). As LOCI parameters, we used a PSF FWHM of 6 pixels, an angular protection zone of 0.7 FWHM, and 200 PSF footprint optimization regions. Individual PSF-subtracted frames were de-rotated and combined using a trimmed mean approach to produce the final image (see Figure 2 for an example). For each final image of a given target, a signal-to-noise (S/N) map was produced by dividing the signal at all positions by the local noise (calculated in an annulus at the corresponding separation). In this process, we include a correction for the signal attenuation imposed by the LOCI algorithm. The S/N map provides a data format in which point sources can be easily identified and in which it can be determined whether or not they

[29] Removal of correlated read-noise, which causes striping in the images.

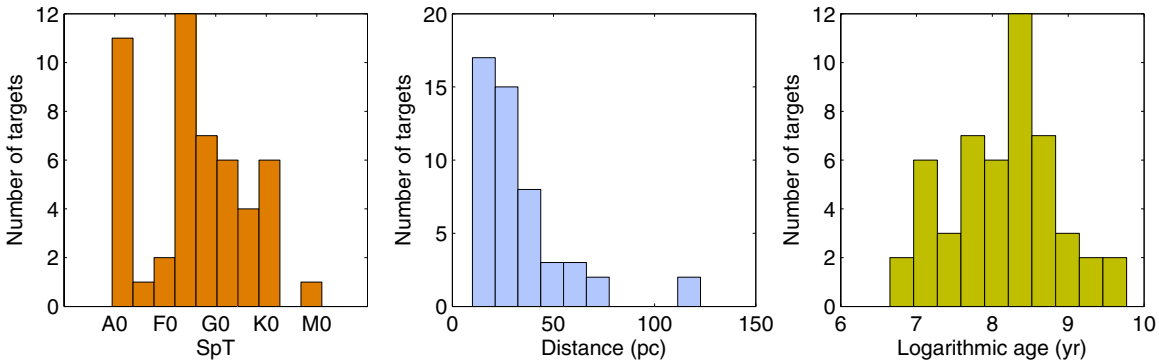

Figure 1. Histograms showing the distributions of the sample in spectral type, distance, and age. The ages plotted here are the geometrical means of the lower and upper age limits derived for each target.

(A color version of this figure is available in the online journal.)

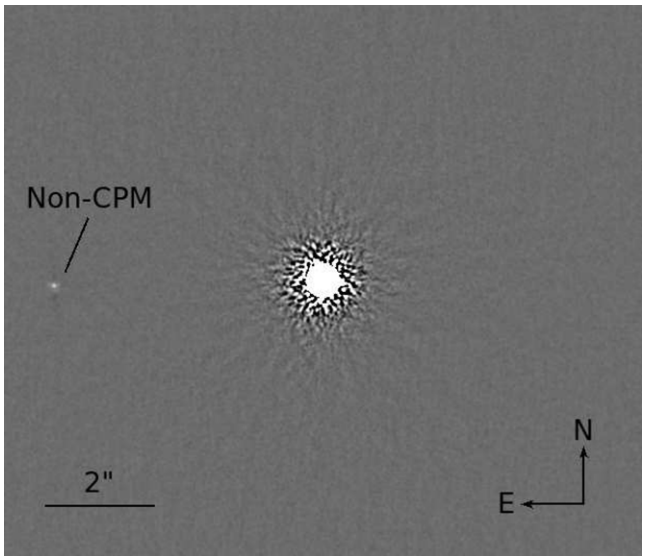

Figure 2. Example of a final reduced image using the ACORNS-ADI pipeline, showing the residual PSF noise of the star HD 113337 and a faint point source to the east. The point source does not share a common proper motion with the primary (abbreviated as non-CPM), hence it is a physically unrelated field object (see Figure 3).

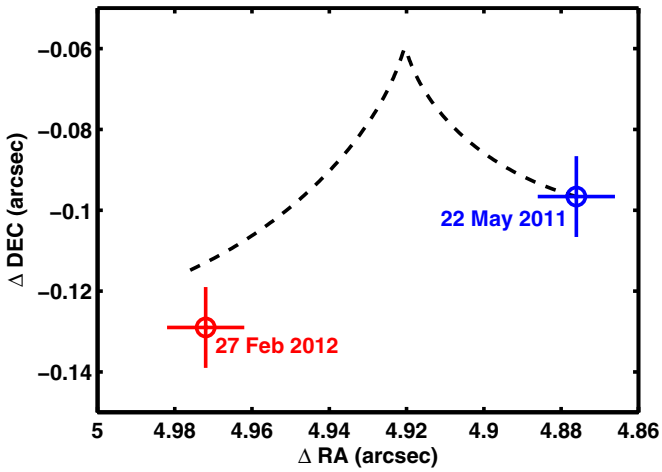

Figure 3. Example of astrometric analysis, for the case of HD 113337. The second epoch observation falls close to the expected motion for a static background object (dashed line), and is clearly inconsistent with common proper motion. Thus, it can be concluded that the point source is physically unrelated to HD 113337.

(A color version of this figure is available in the online journal.)

are statistically significant. Detection limits for a 5.5σ criterion were produced by normalizing the radial noise profiles by the primary brightness, which was determined from non-saturated exposures acquired before and after each ADI sequence.

In cases where candidates were present in the HiCIAO images and the targets had been previously observed with AO-assisted imagers, we analyzed the archival images using similar procedures as above, but adapted to the respective telescopes and instruments. Images from Gemini/NIRI (Hodapp et al. 2003), Gemini/NICI (e.g., Artigau et al. 2008), Keck/NIRC2 (e.g., McLean & Sprayberry 2003), Subaru/IRCS (Kobayashi et al. 2000) and *HST*/NICMOS (e.g., Schultz et al. 2003) were used for this purpose, saving several hours of Subaru telescope time that would otherwise have been necessary for executing follow-up observations in those cases, and thus demonstrating the broad utility of archiving data from large telescopes.

4. RESULTS

4.1. General Results

As can be generally expected in a survey of this kind, many faint point sources are detected in the images, the majority of which are physically unrelated background stars. Due to the fact that the contaminant fraction increases rapidly with angular separation from the parent star, small angular separations have been prioritized for follow-up. Companion candidates that were detected in the data inside of 5″ and with a >5.5σ significance were checked for common proper motion by either using archival data when available, or second epoch observations over a ∼1 yr baseline (see Figure 3 for an example). No substellar companions have been verified so far among the targets. One target remains for which candidates inside of the priority region have not yet been followed up; HD 162917 was observed in late 2012 and will be re-observed at a later stage. Given the low galactic latitude of this target, the candidates are likely to be background stars. The point sources are listed in Table 2.

In some cases, the debris disk itself could be spatially resolved in our images. Two of these detections have been analyzed in particular detail and published separately: HR 4796 A (Thalmann et al. 2011) and HIP 79977 (Thalmann et al. 2013). Three other targets for which secure disk detections could be made are HD 15115, AU Mic, and HD 141569. These cases are discussed in the individual notes below. The disk detection space of our survey has a very good complementarity to that of the *Hubble Space Telescope* (*HST*). *HST* is able to

Table 1
Observing Log

HD ID	HIP ID	Alt ID	R.A. (hh mm ss)	Decl. (dd mm ss)	N_f[a]	t_{tot}[a] (minutes)	Rot[a] (deg)	Date
HD 377	HIP 682	...	00 08 25.7455	+06 37 00.498	31	10.3	9.28	2010 Dec 2
HD 7590	HIP 5944	V445 And	01 16 29.2530	+42 56 21.911	87	11.6	33.8	2011 Sep 4
HD 8907	HIP 6878	...	01 28 34.3597	+42 16 03.677	86	30.1	33.6	2012 Jan 2
HD 9672	HIP 7345	49 Cet	01 34 37.7788	−15 40 34.893	195	32.5	26.2	2011 Dec 24
HD 10008	HIP 7576	EX Cet	01 37 35.4661	−06 45 37.525	65	10.8	32.8	2010 Dec 2
HD 12039	HIP 9141	DK Cet	01 57 48.9784	−21 54 05.345	270	45.0	21.5	2012 Sep 11
HD 15115	HIP 11360	...	02 26 16.2447	+06 17 33.188	306	28.4	51.3	2009 Dec 25
HD 15115	...	...	...	...	290	6.7	45.4	2009 Dec 25
HD 15745	HIP 11847	...	02 32 55.8103	+37 20 01.045	57	19.0	25.7	2011 Sep 6
HD 17925	HIP 13402	EP Eri	02 52 32.1287	−12 46 10.972	82	8.2	26.0	2011 Sep 6
HD 25457	HIP 18859	HR 1249	04 02 36.745	−00 16 08.12	840	21.0	37.1	2012 Sep 13
HD 281691	...	V1197 Tau	04 09 09.7402	+29 01 30.345	940	156.7	79.1	2012 Nov 7
HD 31295	HIP 22845	7 Ori	04 54 53.7279	+10 09 02.999	213	5.3	27.5	2011 Nov 20
HD 40136	HIP 28103	η Lep	05 56 24.2930	−14 10 03.719	780	19.5	27.9	2012 Nov 5
HD 60737	HIP 37170	...	07 38 16.4417	+47 44 55.230	71	17.8	19.3	2012 Jan 1
HD 69830	HIP 40693	LHS 245	08 18 23.9473	−12 37 55.824	159	14.8	26.7	2010 Jan 23
HD 70573	...	V748 Hya	08 22 49.951	+01 51 33.55	66	16.5	44.6	2011 Jan 30
HD 73350	HIP 42333	V401 Hya	08 37 50.2932	−06 48 24.786	400	33.3	25.5	2011 Dec 30
HD 73752	HIP 42430	LHS 5139A	08 39 07.9003	−22 39 42.750	231	9.6	12.0	2011 Mar 25
HD 72905	HIP 42438	3 Uma	08 39 11.7040	+65 01 15.264	7742	193.6	17.3	2011 Dec 24
HD 76151	HIP 43726	NLTT 20504	08 54 17.9475	−05 26 04.054	640	16.0	27.9	2011 Dec 26
HD 88215	HIP 49809	HR 3991	10 10 05.8864	−12 48 57.324	510	21.3	21.3	2011 Dec 31
HD 91312	HIP 51658	HR 4132	10 33 13.8883	+40 25 32.016	750	18.8	35.0	2012 May 12
HD 92945	HIP 52462	V419 Hya	10 43 28.2717	−29 03 51.421	79	13.2	16.5	2011 Dec 25
HD 102647	HIP 57632	β Leo	11 49 03.5776	+14 34 19.417	82	1.9	115.0	2010 Jan 24
HD 104860	HIP 58876	...	12 04 33.7302	+66 20 11.720	64	21.3	20.8	2012 Apr 11
HD 106591	HIP 59774	δ Uma	12 15 25.5601	+57 01 57.421	250	11.6	23.5	2010 Jan 25
HD 106591	...	...	...	...	369	9.2	22.8	2011 Jan 28
HD 107146	HIP 60074	NLTT 30317	12 19 06.5015	+16 32 53.869	160	37.1	34.3	2009 Dec 24
HD 107146	...	...	...	...	246	20.5	122.3	2011 Mar 25
HD 109085	HIP 61174	η Crv	12 32 04.2270	−16 11 45.627	71	4.9	21.3	2010 Jan 23
HD 109573	HIP 61498	HR 4796A	12 36 01.0316	−39 52 10.219	87	14.5	23.5	2011 May 24
HD 110411	HIP 61960	ρ Vir	12 41 53.0565	+10 14 08.251	183	7.6	63.0	2011 Jan 29
HD 112429	HIP 63076	IR Dra	12 55 28.5486	+65 26 18.505	258	6.5	20.6	2011 May 24
HD 113337	HIP 63584	HR 4934	13 01 46.9269	+63 36 36.810	159	13.3	19.0	2011 May 21
HD 113337	...	...	...	...	174	14.5	20.0	2012 Feb 27
HD 125162	HIP 69732	NLTT 36818	14 16 23.0187	+46 05 17.900	225	7.5	28.6	2011 Jan 30
HD 127821	HIP 70952	NLTT 37640	14 30 46.0702	+63 11 08.836	130	10.8	18.9	2011 May 26
HD 128167	HIP 71284	σ Boo	14 34 40.8171	+29 44 42.468	730	18.3	75.3	2012 Apr 11
HD 128311	HIP 71395	HN Boo	14 36 00.5607	+09 44 47.466	180	15.0	66.2	2012 Feb 27
HD 135599	HIP 74702	V379 Ser	15 15 59.1667	+00 47 46.905	198	13.9	42.6	2011 May 25
HD 135599	...	...	...	...	231	19.3	54.6	2012 Feb 28
HD 139006	HIP 76267	α CrB	15 34 41.2681	+26 42 52.895	460	11.5	83.5	2012 Apr 12
HD 139664	HIP 76829	NLTT 40843	15 41 11.3774	−44 39 40.338	240	6.0	15.5	2011 May 22
HD 141569	HIP 77542	...	15 49 57.7489	−03 55 16.360	74	12.3	33.2	2011 Mar 26
HD 146897	HIP 79977	...	16 19 29.2425	−21 24 13.264	60	20.0	19.6	2012 May 12
HD 146897	...	...	...	...	69	34.5	18.3	2012 Jul 7
HD 152598	HIP 82587	53 Her	16 52 58.0578	+31 42 06.026	630	21.0	43.0	2012 May 11
HD 161868	HIP 87108	γ Oph	17 47 53.5605	+02 42 26.194	800	20.0	41.3	2012 Jul 11
HD 162917	HIP 87558	HR 6670	17 53 14.1849	+06 06 05.127	243	17.0	57.4	2012 Jul 9
HD 175742	HIP 92919	V775 Her	18 55 53.2247	+23 33 23.940	87	14.5	104.3	2011 May 23
HD 175742	...	...	...	...	222	37.0	123.8	2012 May 11
HD 183324	HIP 95793	V1431 Aql	19 29 00.9882	+01 57 01.611	276	36.8	34.7	2012 Jul 10
HD 192263	HIP 99711	V1703 Aql	20 13 59.846	−00 52 00.75	77	12.8	44.1	2012 May 14
HD 197481	HIP 102409	AU Mic	20 45 09.5318	−31 20 27.238	53	25.8	11.7	2009 Nov 1
HD 206860	HIP 107350	HN Peg	21 44 31.3299	+14 46 18.981	207	8.6	72.1	2011 Aug 3
HD 207129	HIP 107649	NLTT 52100	21 48 15.7514	−47 18 13.014	232	5.8	16.6	2011 Aug 2

Note. [a] N_f denotes the number of frames used, t_{tot} the total integration time, and θ_r the field rotation angle during the observation.

observe at visible wavelengths with exquisite sensitivity and has a PSF that is unaffected by the atmosphere, which means that it can observe faint and smooth disk emission. Such emission is much more difficult to observe from the ground, since our near-infrared observations are more sensitivity limited, in addition to the fact that PSF variations due to varying seeing are very similar in their characteristics to smooth disk material. In addition, this study has made use of ADI, which benefits

Table 2
Properties of the Imaged Point Sources

HD ID	CC	ΔH (mag)	Δ R.A. ($''$)	Δ Decl. ($''$)	Epoch
HD 15745	1	11.1 ± 0.1	-1.85 ± 0.01	-0.63 ± 0.01	2011 Sep 6
HD 60737	1	10.3 ± 0.1	6.29 ± 0.01	-3.02 ± 0.01	2012 Jan 1
HD 69830	1	13.4 ± 0.1	-5.73 ± 0.01	-3.91 ± 0.01	2010 Jan 23
HD 70573	1	13.8 ± 0.2	2.61 ± 0.01	-2.24 ± 0.01	2011 Jan 30
HD 73350	1	11.7 ± 0.1	2.90 ± 0.01	5.23 ± 0.01	2011 Dec 30
HD 73752	1	1.2 ± 0.1	0.67 ± 0.01	0.80 ± 0.01	2011 Mar 25
HD 73752	2	13.7 ± 0.1	-4.50 ± 0.01	6.02 ± 0.01	2011 Mar 25
HD 88215	1	14.5 ± 0.1	-7.47 ± 0.01	-0.89 ± 0.01	2011 Dec 31
HD 104860	1	12.1 ± 0.1	-3.10 ± 0.01	-0.55 ± 0.01	2012 Apr 11
HD 106591	1	15.1 ± 0.1	3.22 ± 0.01	-1.25 ± 0.01	2010 Jan 25
HD 106591	1	15.1 ± 0.1	3.08 ± 0.01	-1.30 ± 0.01	2011 Jan 28
HD 106591	2	15.9 ± 0.1	1.26 ± 0.01	-5.57 ± 0.01	2010 Jan 25
HD 106591	2	16.1 ± 0.2	1.06 ± 0.01	-5.59 ± 0.01	2011 Jan 28
HD 107146	1	14.9 ± 0.1	-3.69 ± 0.01	-5.07 ± 0.01	2011 Mar 25
HD 113337	1	13.6 ± 0.1	4.88 ± 0.01	-0.10 ± 0.01	2011 May 21
HD 113337	1	13.4 ± 0.1	4.97 ± 0.01	-0.13 ± 0.01	2012 Feb 27
HD 128311	1	12.4 ± 0.1	4.33 ± 0.01	-6.38 ± 0.01	2012 Feb 27
HD 141569	1	2.2 ± 0.1	-5.50 ± 0.01	5.23 ± 0.01	2011 Mar 26
HD 161868	1	14.2 ± 0.1	-6.10 ± 0.01	-0.10 ± 0.01	2012 Jul 11
HD 161868	2	14.8 ± 0.1	6.05 ± 0.01	3.89 ± 0.01	2012 Jul 11
HD 162917	1	12.0 ± 0.1	2.46 ± 0.01	-1.67 ± 0.01	2012 Jul 9
HD 162917	2	12.5 ± 0.1	-2.73 ± 0.01	2.06 ± 0.01	2012 Jul 9
HD 162917	3	12.8 ± 0.1	0.35 ± 0.01	-4.41 ± 0.01	2012 Jul 9
HD 175742	1	10.6 ± 0.1	1.72 ± 0.01	1.97 ± 0.01	2011 May 23
HD 175742	1	10.8 ± 0.1	1.59 ± 0.01	2.24 ± 0.01	2012 May 11
HD 183324	1	13.7 ± 0.1	-0.73 ± 0.01	1.71 ± 0.01	2012 Jul 10
HD 183324	2	14.6 ± 0.1	3.25 ± 0.01	1.36 ± 0.01	2012 Jul 10
HD 183324	3	14.6 ± 0.1	3.40 ± 0.01	-1.16 ± 0.01	2012 Jul 10
HD 183324	4	13.6 ± 0.1	1.49 ± 0.01	-4.29 ± 0.01	2012 Jul 10
HD 183324	5	13.9 ± 0.1	-4.44 ± 0.01	-3.15 ± 0.01	2012 Jul 10
HD 183324	6	15.2 ± 0.2	5.00 ± 0.01	4.43 ± 0.01	2012 Jul 10
HD 192263	1	13.6 ± 0.1	-4.41 ± 0.01	-5.83 ± 0.01	2012 May 14
HD 206860	1	15.3 ± 0.2	1.69 ± 0.01	2.45 ± 0.01	2011 Aug 3
HD 281691	1	1.7 ± 0.1	4.33 ± 0.01	5.22 ± 0.01	2012 Nov 7

the detection of sharp features in the disk while strongly self-subtracting smooth emission, particularly if it is azimuthally symmetric. On the other hand, the high contrast and spatial resolution of HiCIAO allows for detection of disks and disk features at small angular separations, where *HST* is unable to provide a comparable performance. Hence, we are unable to detect large-scale, smooth, and low-inclination structures such as the second ring of the HD 141569 disk, but can provide novel results on small-scale, sharp and high-inclination features such as the inner region of the HIP 79977 disk.

The contrast performances for point sources are shown in Figure 4 and listed in Table 3. The achievable contrast is largely dependent on the field rotation during an observation. This is due to the connection between field rotation and ADI performance. An increased total field rotation benefits ADI because it maximizes the number of reference frames in which the planet signature is sufficiently separated from its location in the target frame to be useful, which helps as long as the number of reference frames does not become so large that the LOCI optimization becomes overconstrained. In our reductions, we avoid this overconstraining by limiting the number of reference frames for each target frame to ~80, uniformly spread across the observing sequence, which we find to produce roughly optimal performance. The contrast depends not only on the total field rotation, but also on the rotation rate. This is caused by the fact that frames taken over a small time span tend to correlate

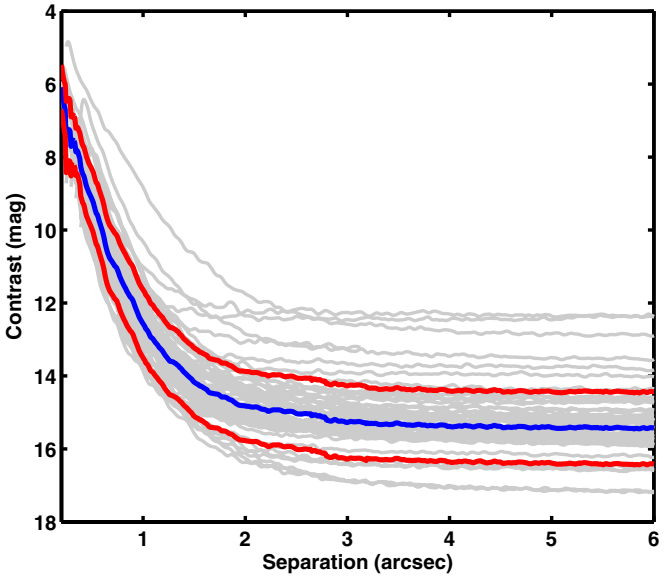

Figure 4. Contrast as a function of angular separation. The individual contrast curves are shown in light gray. The thick blue line denotes the median contrast, and the red lines are separated from the median by one standard deviation of the curve-to-curve scatter in each direction. The target LHS 5139, where the binary companion affects the azimuthally averaged contrast to a significant extent, has been omitted from the figure.

(A color version of this figure is available in the online journal.)

better than frames taken over larger time spans. A larger rotation rate thus allows for the use of reference frames that are better correlated with the target frame. The rotation rate that can be acquired depends on the declination of the target—a minimal $|\delta - l|$ provides a maximal rotation rate, where δ is the declination and l the latitude of the telescope.

4.2. Individual Targets

Below, we list individual notes concerning the results on different targets in the survey, such as detections of disks or point sources, as well as other details from the scientific literature that are relevant for the context.

HD 15115 (HIP 11360). This star has a known debris disk that has been spatially resolved at several near-infrared wavelengths (e.g., Kalas et al. 2007b; Debes et al. 2008; Rodigas et al. 2012). We also detect the disk in the HiCIAO data (see Figure 5), but at limited S/N which does not improve on the results in previous studies.

HD 15745 (HIP 11847). The debris disk around HD 15745 has been spatially resolved in *HST* observations (Kalas et al. 2007a), but is not visible in the HiCIAO images due to its smooth and azimuthally extended features. A candidate companion was seen at $\Delta\alpha = -1\farcs85$ and $\Delta\delta = -0\farcs63$ with HiCIAO. The point source is faint but visible in the archival *HST* images from 2004, where it has $\Delta\alpha = -1\farcs65$ and $\Delta\delta = -0\farcs89$, demonstrating that it is a background contaminant. There is also an intermediate epoch available from Keck in 2007, with the point source located at $\Delta\alpha = -1\farcs72$ and $\Delta\delta = -0\farcs75$, further confirming this conclusion.

HD 60737 (HIP 37170). The field of HD 60737 is empty except for a point source at $\Delta\alpha = 6\farcs29$ and $\Delta\delta = -3\farcs02$, which has already been identified as a background star by Metchev & Hillenbrand (2009).

HD 69830 (HIP 40693, LHS 245). This system is notable for its planetary system which contains three known planets so far,

Table 3
Contrast at a Range of Angular Separations

HD ID	Ep.	0.″25 (mag)	0.″5 (mag)	0.″75 (mag)	1.″0 (mag)	1.″5 (mag)	2.″0 (mag)	3.″0 (mag)	5.″0 (mag)
HD 377	1	...	...	9.6	11.3	12.9	13.9	14.1	14.3
HD 7590	1	...	8.8	10.7	12.4	14.0	14.6	15.0	15.2
HD 8907	1	7.8	9.5	11.5	13.1	14.7	15.3	15.6	15.7
HD 9672	1	...	8.7	10.3	11.6	13.2	13.9	14.4	14.6
HD 10008	1	7.0	8.8	10.6	12.1	13.8	14.4	14.7	14.9
HD 12039	1	...	8.7	10.7	12.1	13.6	14.1	14.4	14.6
HD 15115	1	5.8	7.8	9.6	11.0	11.9	12.2	12.3	12.4
HD 15115	2	7.1	9.3	11.4	12.9	14.0	14.3	...	...
HD 15745	1	7.6	9.2	11.2	12.7	14.1	14.5	14.9	15.0
HD 17925	1	...	8.8	10.8	12.3	14.2	15.1	15.6	15.8
HD 25457	1	...	9.4	11.2	12.9	14.3	14.8	15.3	15.4
HD 281691	1	7.4	9.7	11.0	11.9	12.2	12.4	12.5	12.5
HD 31295	1	5.0	6.5	7.7	8.8	10.6	11.8	12.6	12.8
HD 40136	1	...	10.4	12.2	13.7	15.4	16.1	16.9	17.1
HD 60737	1	...	8.7	10.8	12.3	13.9	14.4	14.8	14.9
HD 69830	1	...	8.7	10.5	11.9	13.7	14.6	14.9	15.1
HD 70573	1	6.5	8.6	10.6	12.0	13.3	13.6	13.9	14.0
HD 73350	1	7.7	9.0	10.7	12.1	13.7	14.6	15.1	15.3
HD 73752	1	...	6.4	6.9	6.8	10.4	12.5	13.8	14.2
HD 72905	1	...	9.0	10.9	12.4	14.1	14.7	15.1	15.2
HD 76151	1	...	8.9	10.6	12.0	13.6	14.3	14.6	14.7
HD 88215	1	...	8.8	11.2	12.7	14.4	15.2	15.6	15.8
HD 91312	1	...	9.3	11.3	12.8	14.6	15.3	15.6	15.7
HD 92945	1	...	7.2	9.0	10.3	12.0	12.9	13.3	13.5
HD 102647	1	...	...	11.8	13.6	15.4	16.3	16.9	17.1
HD 104860	1	...	10.3	12.2	13.6	14.8	15.2	15.4	15.7
HD 106591	1	...	8.9	11.5	13.1	15.1	16.0	16.4	16.5
HD 106591	2	...	9.5	11.4	12.9	15.1	15.8	16.3	16.5
HD 107146	1	6.9	8.8	10.8	12.4	13.8	14.4	...	...
HD 107146	2	7.5	9.1	11.0	12.5	14.2	14.8	15.0	15.1
HD 109085	1	...	...	10.8	12.3	14.1	15.0	15.4	15.8
HD 109573	1	...	9.8	11.5	12.4	14.6	15.2	15.6	15.7
HD 110411	1	...	8.8	10.7	12.1	14.2	15.0	15.4	15.5
HD 112429	1	...	9.4	11.3	13.0	14.6	15.1	15.4	15.6
HD 113337	1	...	9.6	11.4	12.9	14.5	15.2	15.5	15.7
HD 113337	2	...	9.8	11.4	12.9	14.5	15.2	15.7	15.7
HD 125162	1	...	7.9	9.6	11.1	13.3	14.3	15.0	15.2
HD 127821	1	...	8.6	10.0	11.4	13.2	14.0	14.5	14.6
HD 128167	1	...	10.1	12.0	13.6	15.2	16.0	16.4	16.5
HD 128311	1	...	9.5	11.4	12.7	14.4	15.0	15.5	15.6
HD 135599	1	8.4	10.7	12.5	13.6	14.9	15.3	15.6	15.6
HD 135599	2	...	10.4	12.6	13.9	15.3	15.7	16.1	16.2
HD 139006	1	...	9.9	12.1	13.7	15.6	16.4	16.9	...
HD 139664	1	...	8.4	10.0	11.5	13.4	14.4	15.2	15.5
HD 141569	1	8.7	9.9	11.9	13.0	14.0	14.4	14.6	14.7
HD 146897	1	...	9.4	11.2	12.2	13.2	13.5	13.7	13.8
HD 146897	2	...	8.4	10.5	11.6	12.7	13.1	13.2	...
HD 152598	1	...	9.6	11.7	13.3	14.6	15.0	15.3	15.4
HD 161868	1	...	9.1	11.0	12.6	14.2	15.0	15.4	15.6
HD 162917	1	...	8.8	10.7	12.1	13.8	14.5	14.8	15.1
HD 175742	1	7.8	10.2	12.1	13.5	14.6	15.0	15.3	15.4
HD 175742	2	...	10.3	12.4	13.8	14.9	15.3	15.5	15.7
HD 183324	1	...	9.7	11.6	13.0	14.3	14.8	15.2	15.3
HD 192263	1	...	10.2	12.1	13.4	14.7	15.1	15.3	15.5
HD 197481	1	...	8.5	11.1	12.5	14.2	14.8	15.5	...
HD 206860	1	...	10.0	12.0	13.5	14.9	15.5	15.7	15.8
HD 207129	1	...	9.2	11.1	12.6	14.2	14.9	15.3	15.4

all with Neptune-like masses (Lovis et al. 2006). It also hosts a warm debris disk (Beichman et al. 2006), which has been resolved with interferometry (Smith et al. 2009). Our images do not reveal the disk, and due to the probably quite old age of the system (approximately 6 Gyr; Mamajek & Hillenbrand 2008) and small physical scale (~1–2 AU) of the dust location, no stringent constraints can be drawn regarding planets near the disk edge from the imaging. We do detect a point source at $\Delta\alpha = -5.''73$ and $\Delta\delta = -3.''91$. This candidate is visible in an archival *HST* image from 2007 with $\Delta\alpha = -5.''24$ and $\Delta\delta = -5.''94$, hence it is a physically unrelated background star.

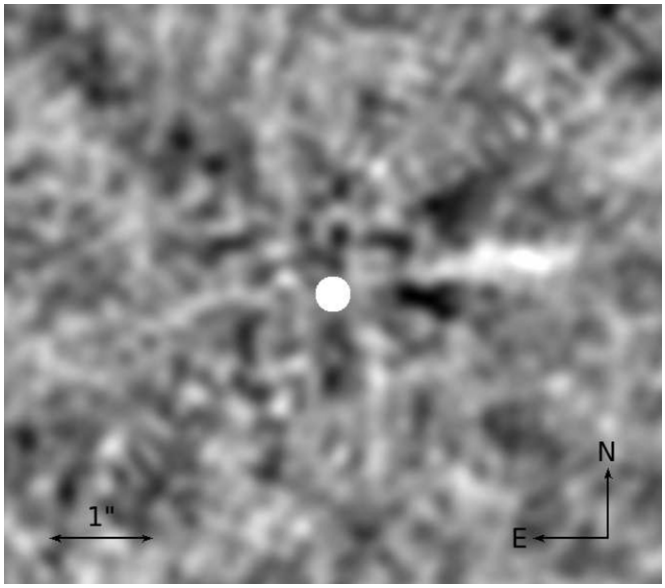

Figure 5. Image of the disk around HD 15115. The S/N is limited, but disk emission is seen at the expected region of maximal disk flux from previous images (compare, e.g., Rodigas et al. 2012), on the western side of the star. A Gaussian smoothing kernel of 15 pixel FWHM has been applied to the data.

HD 70573 (V748 Hya). There is an object at $\Delta\alpha = 2.''61$ and $\Delta\delta = -2.''24$ in the HiCIAO images. Although the source appears somewhat extended, we nonetheless examined archival data to test its nature. This turned up the object in archival NICI images, where it is located at $\Delta\alpha = 2.''47$ and $\Delta\delta = -2.''38$, indeed, implying non-common proper motion. This star has a planet candidate from radial velocity measurements, at a semi-major axis of 1.8 AU (Setiawan et al. 2007).

HD 73350 (HIP 42333, V401 Hya). There is a point source at $\Delta\alpha = 2.''90$ and $\Delta\delta = 5.''23$ in the HiCIAO data. It is considered of low priority due to its relatively large separation from the primary.

HD 73752 (HIP 42430, LHS 5139). A known binary (e.g., Mason et al. 2001), the location of the secondary relative to the primary in the HiCIAO images is $\Delta\alpha = 0.''67$ and $\Delta\delta = 0.''80$. There is another possible candidate in the image at $\Delta\alpha = -4.''50$ and $\Delta\delta = 6.''02$, but it is just at the edge of the detector, hence it is considered of low priority.

HD 88215 (HIP 49809, HR 3991). An extended source is present at $\Delta\alpha = -7.''47$ and $\Delta\delta = -0.''89$, which is probably a background galaxy.

HD 92945 (HIP 52462, V419 Hya). The debris disk around HD 92945 has been recently spatially resolved with *HST* (Golimowski et al. 2011). It is not visible in the HiCIAO images.

HD 104860 (HIP 58876). The only point source in the field of HD 104860 is located at $\Delta\alpha = -3.''10$ and $\Delta\delta = 0.''55$, and has already been identified as a background star in Metchev & Hillenbrand (2009).

HD 106591 (HIP 59774, δ Uma). This star was observed in two separate epochs. Two point sources are present in the images. The brighter of the candidates resides at $\Delta\alpha = 3.''22$ and $\Delta\delta = -1.''25$ in the first epoch and $\Delta\alpha = 3.''08$ and $\Delta\delta = -1.''30$

in the second epoch. The fainter one is located at $\Delta\alpha = 1\farcs26$ and $\Delta\delta = -5\farcs57$ in the first epoch and $\Delta\alpha = 1\farcs06$ and $\Delta\delta = -5\farcs59$ in the second epoch. Neither is therefore physically bound to HD 106591. The brighter candidate however displays a peculiar astrometric behavior, with a deviation of close to 100 mas from the trajectory of a static background star over a baseline of one year. This could imply that it is a field brown dwarf at a similar distance as HD 106591, or otherwise that it is a distant background star with an anomalously high proper motion.

HD 107146 (HIP 60074, NLTT 30317). The debris disk around HD 107146 has been spatially resolved in the past (e.g., Ardila et al. 2004; Ertel et al. 2011), but since it is smooth and has a nearly face-on orientation, it is not visible in the HiCIAO images. An object is visible at $\Delta\alpha = -3\farcs69$ and $\Delta\delta = -5\farcs07$, which has been classified as a background galaxy in Ertel et al. (2011).

HD 109573 (HR 4796 A, HIP 61498). As described in Thalmann et al. (2011), we have spatially resolved the disk in this system using ADI, which enabled us to confirm and strengthen conclusions from previous studies of the system (e.g., Schneider et al. 1999, 2009), such as the fact that the disk has a non-zero eccentricity. As is also shown in Thalmann et al. (2011), a planet near the gap edge (coplanar with the disk) would have been detectable at a mass of $\sim$3 $M_{\rm Jup}$ at maximum projected separation, but at minimum projected separation the upper limit is much softer ($\sim$17 $M_{\rm Jup}$) due to the relatively high inclination of the target.

HD 113337 (HIP 63584, HR 4934). There are two epochs of observation available for HD 113337 from HiCIAO, due to the presence of a companion candidate in the data. The candidate has $\Delta\alpha = 4\farcs88$ and $\Delta\delta = -0\farcs10$ in the first epoch and $\Delta\alpha = 4\farcs97$ and $\Delta\delta = -0\farcs13$ in the second epoch, which demonstrates that it is a background star. Furthermore, archival data from NIRC2 in 2010 places the candidate at $\Delta\alpha = 4\farcs74$ and $\Delta\delta = -0\farcs07$, further strengthening this conclusion.

HD 128311 (HIP 71395, HN Boo). The single candidate that can be seen in the HiCIAO field at $\Delta\alpha = 4\farcs33$ and $\Delta\delta = -6\farcs38$ has been established as a background star in Heinze et al. (2010).

HD 139664 (HIP 76829, NLTT 40843). A spatially resolved scattered light *HST* image of the debris disk around HD 139664 exists (Kalas et al. 2006). Although the disk has a high inclination, it appears that it was too faint to be detectable in the HiCIAO images.

HD 141569 (HIP 77542). Despite the fact that the disk around HD 141569 is smooth and has a relatively low inclination, it is nonetheless visible in our HiCIAO images (see Figure 6) due to the high surface brightness. As expected, the S/N is lower than in *HST* images of the target (Clampin et al. 2003). For point sources on the other hand, HiCIAO provides strong limits, with sensitivity down to 1 $M_{\rm jup}$ planets in the sensitivity-limited region. The already known binary companion (Weinberger et al. 2000) is present toward the edge of the field of view.

HD 146897 (HIP 79977). This USco (Upper Scorpius OB association) member has a debris disk (Chen et al. 2006), which was spatially resolved for the first time with HiCIAO, as we reported in Thalmann et al. (2013). The disk has an inner gap within $\sim$40 AU (Chen et al. 2011), but owing to the large distance of 123 pc to the target (van Leeuwen 2007), the gap itself cannot be confidently distinguished in the existing data, and any giant planet that might be responsible for the gap would have been easily missed, particularly since the disk orientation is close to edge-on.

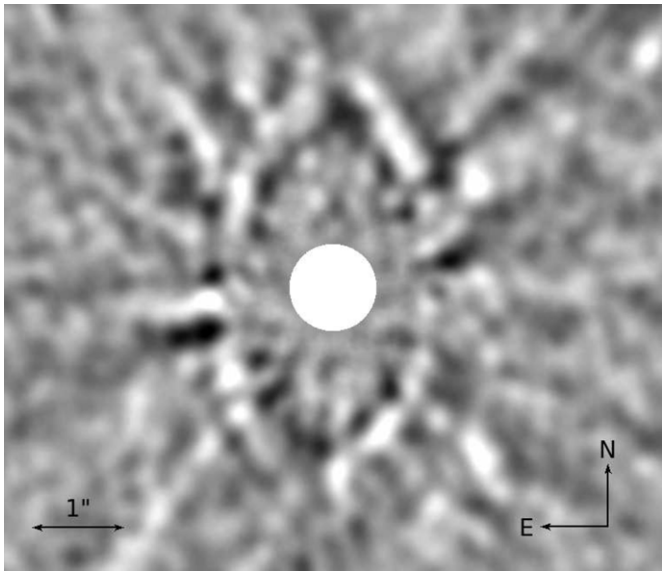

Figure 6. Image of the disk around HD 141569. A Gaussian smoothing kernel of 20 pixel FWHM has been applied to the data. Apparent point sources in the image are due to this smoothing. The image is a zoom-in of the central region to more clearly show the disk structure; the binary companion that is present in the full field of view is therefore not visible in this image.

HD 161868 (HIP 87108, γ Oph). The star γ Oph is in a relatively crowded field with several background stars, although all are outside of 5″ separation. The HiCIAO image is relatively shallow and does not reveal as many candidates as archival NICI data from 2009. However, there are two candidates that overlap between the two data sets. One candidate has $\Delta\alpha = -6\farcs10$ and $\Delta\delta = -0\farcs10$ in the HiCIAO data and $\Delta\alpha = -6\farcs18$ and $\Delta\delta = -0\farcs29$ in the NICI data, and the other has $\Delta\alpha = 6\farcs05$ and $\Delta\delta = 3\farcs89$ in the HiCIAO data and $\Delta\alpha = 5\farcs95$ and $\Delta\delta = 3\farcs63$ in the NICI data. As expected from the large separations, both candidates are background stars.

HD 175742 (HIP 92919, V775 Her). There is an object in the field which, judging by its morphology, is probably a close background binary star. It has been observed in two HiCIAO epochs with $\Delta\alpha = 1\farcs72$ and $\Delta\delta = 1\farcs97$ in the first epoch and $\Delta\alpha = 1\farcs59$ and $\Delta\delta = 2\farcs24$ in the second, confirming its physically unrelated status. In addition, there is an archival epoch from NIRC2 in 2010 where the candidate is located at $\Delta\alpha = 1\farcs90$ and $\Delta\delta = 1\farcs81$, further strengthening this conclusion.

HD 183324 (HIP 95793, V1431 Aql). The brightest and closest companion candidate to HD 183324 has been observed several times with 8 m class telescopes. In the HiCIAO data, it is located at $\Delta\alpha = -0\farcs73$ and $\Delta\delta = 1\farcs71$. In archival *H*-band Keck/NIRC2 images from 2010, it is located at $\Delta\alpha = -0\farcs73$ and $\Delta\delta = 1\farcs63$. The motion clearly demonstrates that the candidate is a physically unrelated background object. There are also three other candidates inside of 5″ in the data: one in the northeast located at $\Delta\alpha = 3\farcs25$ and $\Delta\delta = 1\farcs36$ in the HiCIAO image and $\Delta\alpha = 3\farcs24$ and $\Delta\delta = 1\farcs29$ in the Keck image, one in the northwest located at $\Delta\alpha = 3\farcs40$ and $\Delta\delta = -1\farcs16$ in the HiCIAO image and $\Delta\alpha = 3\farcs40$ and $\Delta\delta = -1\farcs20$ in the Keck image, and one toward the south located at $\Delta\alpha = 1\farcs49$ and $\Delta\delta = -4\farcs29$ in the HiCIAO image and $\Delta\alpha = 1\farcs50$ and $\Delta\delta = -4\farcs35$ in the Keck image. Hence, all of these are also physically unrelated to the target star.

HD 192263 (HIP 99711, V1703 Aql). Aside from its debris disk, HD 192263 also hosts a planet candidate detected through

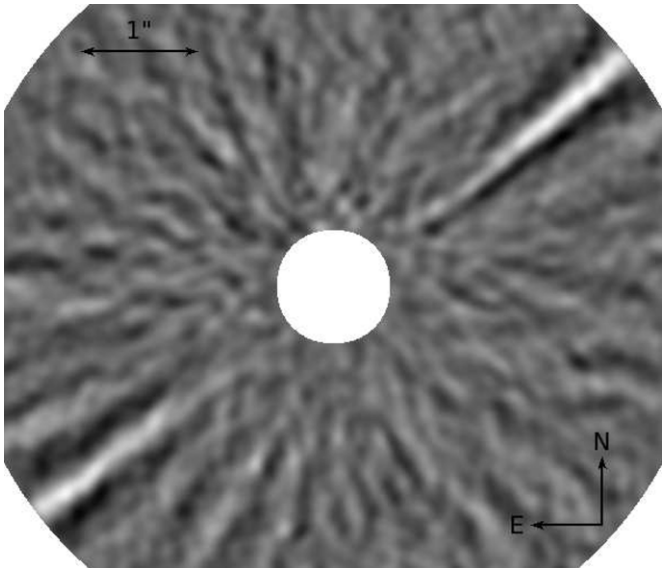

Figure 7. Image of the disk around AU Mic. The characteristic edge-on disk spans diagonally from the southeast to the northwest. The image was acquired with the regular LOCI-based ADI procedure, which causes the black shadows seen on both sides of the disk. A Gaussian smoothing kernel of 10 pixel FWHM has been applied to the data.

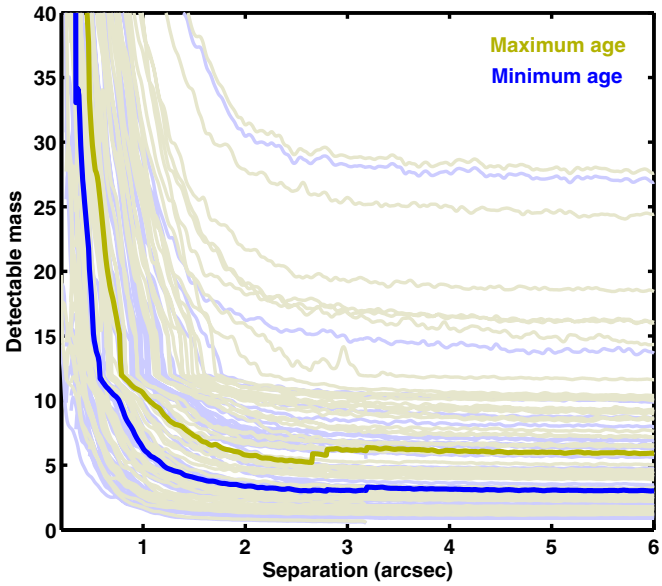

Figure 8. Detectable mass as a function of angular separation, based on the COND/DUSTY models. The blue curves correspond to the mass at the lower limit of the age range estimated for each target, and the gold curves correspond to the mass at the upper limit. The thick opaque lines are the median mass detection limits across the sample, and the lighter narrower lines are the individual cases. (A color version of this figure is available in the online journal.)

radial velocity (e.g., Santos et al. 2003). In Chauvin et al. (2006), it is mentioned that several candidates have been discovered and confirmed to be background stars in NACO images of HD 192263. We observe one of these objects within the HiCIAO field of view at $\Delta\alpha = -4\farcs41$ and $\Delta\delta = -5\farcs83$, and otherwise no new objects.

HD 197481 (HIP 102409, AU Mic). Best known as AU Mic, this star has a well known debris disk which shows up clearly in our data (see Figure 7). The field of view is smaller than for most stars in our sample, due to the PDI setting that was used for this observation (see Section 3).

HD 206860 (HIP 107350, HN Peg). A candidate is visible at $\Delta\alpha = 1\farcs69$ and $\Delta\delta = 2\farcs45$. We retrieved the companion in NIRI data from 2006, where the candidate is located at $\Delta\alpha = 2\farcs91$ and $\Delta\delta = 1\farcs93$, consistent with a background star.

HD 207129 (HIP 107649, NLTT 52100). Spatially resolved images in scattered light of HD 207129 have been acquired with *HST* (Krist et al. 2010). It is spatially extended and very faint, and hence, as expected, it is invisible in the HiCIAO images.

HD 281691 (V1197 Tau). We observe a previously known companion in the HiCIAO images at $\Delta\alpha = 4\farcs33$ and $\Delta\delta = 5\farcs22$, which was first discovered by Köhler & Leinert (1998) and has been confirmed by Metchev & Hillenbrand (2009).

5. DISCUSSION

Both the β Pic and HR 8799 systems have debris disks with gaps or cavities in them, and directly imaged planets that are consistent with being responsible for carving these features. Given that we are sensitive to similar mass planets in our observations, and given that we have constraints on the semi-major axis space where the gaps originate from the spectral energy distributions (SEDs) of the targets, it is possible to address to which extent similarly massive planets are responsible for debris disk gaps in general. Given the many caveats involved in such a study, however, such an analysis should be treated with caution.

One primary issue in the analysis is the uncertainty in the location of the gap. It is possible to constrain the spatial distribution of the circumstellar dust from the SED by constraining the temperature, but since only a very limited number of data points are available in general, there are ambiguities between the location and the radiative properties of the dust. In this study, we adopt values of $a_{\rm dust}$ from the literature based on the global assumption that the dust grains emit like blackbodies. How the resulting physical separation relates to the semi-major axis of a given hypothetical shepherding planet in the system is another complex uncertainty. Here, we simply take the $a_{\rm dust}$ itself to represent the physical scale around which we wish to evaluate the presence or absence of a planet; the motivation being that the dominating disk flux should arise close to the inner edge (since that is where the dust is hottest and, in general, most dense) and that the planet responsible for carving the gap should be close to the edge. This is not necessarily relevant if, for instance, there are multiple planets responsible for the gap. With regards to planet detectability near the gap, the gap locations adopted here are probably very conservative, as can be seen in Booth et al. (2013). In all cases studied by Booth et al. (2013) where the real gap location could be observed, the real location is never smaller than the blackbody prediction, but is often larger by a factor two.

We derive mass detection limits from the contrast curves using COND- and DUSTY-based evolutionary models (Chabrier et al. 2000; Allard et al. 2001; Baraffe et al. 2003) and the age limits in Table 4 (see Figure 8). COND was used whenever the predicted temperature was below 1700 K, and DUSTY when it was above this limit. These "hot-start" models may overpredict the brightness for a given mass and age if the initial entropy is lower than assumed in those models (see, e.g., Spiegel & Burrows 2012). However, the exoplanets that have been discovered to date are consistent with hot-start conditions and exclude at least the coldest ranges of initial conditions (e.g., Janson et al. 2011; Bonnefoy et al. 2013; Marleau & Cumming 2013). Furthermore,

Table 4
Target Properties

HD ID	SpT	H (mag)	Dist. (pc)	τ_l[a] (Myr)	τ_u[a] (Myr)	τ Ref[b]	a_{dust}[c] (AU)	a Ref[b]	f_y[d] (%)	f_o[d] (%)	$m_{s,y}$[e] (M_{jup})	$m_{s,o}$[e] (M_{jup})
HD 377	G2	6.15	39.1	25	220	A08	10	H08	0.0	0.0	2	6
HD 7590	G0	5.26	23.2	420	500	P09	49	P09	84.1	74.8	7	8
HD 8907	F8	5.49	34.8	100	400	MH09	61	R07	94.4	74.6	3	7
HD 9672	A1	5.53	59.4	30	50	Z12	59	R07	66.1	35.0	3	4
HD 10008	G5	5.90	24.0	150	300	L07	9	P09	0.0	0.0	3	5
HD 12039	G4	6.56	40.9	20	50	Z04	8	C09	0.0	0.0	1	2
HD 15115	F2	5.86	45.2	10	14	M11	35	R07	91.1	89.6	1	1
HD 15745	F2	6.61	63.5	10	14	M11	22	R07	21.7	13.0	1	1
HD 17925	K1.5	4.23	10.4	40	130	L07	4	H08	12.1	0.0	1	2
HD 25457	F5	4.34	18.8	50	100	L06, J07	15	R07	71.2	39.2	2	3
HD 31295	A0	4.52	35.7	10	100	R05, R07	47	R07	64.8	0.0	3	10
HD 40136	F2	2.99	14.9	300	1410	B06, R07	6	R07	0.0	0.0	4	11
HD 60737	G0	6.31	39.3	80	320	C09	35	C09	61.3	8.0	3	6
HD 69830	G8	4.36	12.5	5700	6100	MH08	1	B11	0.0	0.0	27	28
HD 70573	G1	7.28	46.0	30	125	A08	28	H08	71.6	4.7	2	4
HD 72905	G1.5	4.28	14.4	50	200	MH09	7	H08	17.2	0.0	2	4
HD 73350	G0	5.32	24.0	370	650	P09	19	P09	0.0	0.0	6	8
HD 73752	G5	3.59	19.4	1600	7180	M10	21	R07	0.0	0.0	25	53
HD 76151	G3	4.63	17.4	1390	1890	V12	6	T08	0.0	0.0	14	16
HD 88215	F2	4.46	27.7	480	1760	C11	5	T08	0.0	0.0	9	16
HD 91312	A7	4.06	34.6	200	420	R07, V12	181	R07	99.4	26.9	7	10
HD 92945	K1.5	5.77	21.4	80	120	L07	24	R07	60.8	36.9	4	5
HD 102647	A3	1.92	11.0	50	520	R05, R07, V12	12	R07	77.1	0.0	2	7
HD 104860	F8	6.58	45.5	20	80	MH09	41	H08	98.8	84.7	1	2
HD 106591	A3	3.31	24.7	300	490	R05, V12	16	R07	0.0	0.0	6	9
HD 107146	G2	5.61	27.5	80	200	A08	27	R07	74.7	46.5	2	3
HD 109085	F2	3.37	18.3	600	1300	L07	5	R07	0.0	0.0	10	15
HD 109573	A0	5.79	72.8	10	14	Z04	33	R07	32.2	19.9	1	1
HD 110411	A0	4.76	36.3	100	500	R07, V12	38	R07	30.8	0.0	4	10
HD 112429	F0	4.60	29.3	50	450	P09	24	P09	54.7	0.0	3	9
HD 113337	F6	5.05	36.9	20	60	M11	18	R07	41.3	0.0	1	3
HD 125162	A0	4.03	30.4	180	320	R05, R07, V12	33	R07	0.0	0.0	7	9
HD 127821	F4	5.10	31.8	170	270	M11	56	R07	71.0	47.4	6	7
HD 128167	F2	3.46	15.8	1000	4780	R07, V12	90	R07	45.7	0.0	10	25
HD 128311	K0	5.30	16.5	140	460	M10	5	T08	0.0	0.0	2	5
HD 135599	K0	5.12	15.8	190	230	P09	11	L09	68.7	64.7	2	3
HD 139006	A0	2.39	23.0	270	500	R05, R07, V12	17	R07	0.0	0.0	4	7
HD 139664	F4	3.73	17.4	150	300	L06	25	R07	57.3	27.7	4	6
HD 141569	B9.5	6.86	116.1	4	5	M04	29	R07	46.7	2.1	1	1
HD 146897	F2	7.85	122.7	5	10	Z99, P12, S12	16	C06	0.0	0.0	1	2
HD 152598	F0	4.54	29.2	140	280	M09	9	R07	0.0	0.0	5	7
HD 161868	A0	3.66	31.5	180	310	R05, R07	59	R07	65.7	14.4	7	9
HD 162917	F4	4.83	31.1	200	800	R07	21	R07	0.0	0.0	6	12
HD 175742	K0	5.76	21.4	40	60	P09	4	P09	0.0	0.0	1	2
HD 183324	A0	5.59	61.2	5	20	R05	18	MW09	3.7	0.0	1	2
HD 192263	K2.5	5.69	19.3	550	570	S05	11	D11	0.0	0.0	6	6
HD 197481	M1	4.83	9.9	10	14	P09	10	R07	94.7	94.7	1	1
HD 206860	G0	4.60	17.9	150	300	L07	7	T08	0.0	0.0	3	4
HD 207129	G0	4.31	16.0	600	3200	R07, MH08	28	R07	34.9	0.0	8	19
HD 281691	G8	8.51	73	10	30	M08	23	C09	74.4	24.8	2	2

Notes.

[a] The lower and upper limits on the age are denoted τ_l and τ_u.

[b] The references are abbreviated as follows: A08: Apai et al. 2008; B06: Beichman et al. 2006; B11: Beichman et al. 2011; C06: Chen et al. 2006; C09: Carpenter et al. 2009; C11: Casagrande et al. 2011; D11: Dodson-Robinson et al. 2011; H08: Hillenbrand et al. 2008; J07: Janson et al. 2007; L06: López-Santiago et al. 2006; L07: Lafrenière et al. 2007a; L09: Lawler et al. 2009; M04: Merín et al. 2004; M08: Meyer et al. 2008; MH08: Mamajek & Hillenbrand 2008; M09: Moór et al. 2009; MH09: Metchev & Hillenbrand 2009; MW09: Morales et al. 2009; M10: Maldonado et al. 2010; M11: Moór et al. 2011; P09: Plavchan et al. 2009; P12: Pecaut et al. 2012; R05: Rieke et al. 2005; R07: Rhee et al. 2007; S05: Saffe et al. 2005; S12: Song et al. 2012; T08: Trilling et al. 2008; V12: Vican 2012; Z99: de Zeeuw et al. 1999; Z04: Zuckerman & Song 2004; Z12: Zuckerman & Song 2012.

[c] Location of the dust, see text for discussion.

[d] Detection probability for a 10 M_{jup} planet at semi-major axis a_{dust}, denoted f_y for the youngest and f_o for the oldest age.

[e] Mass limits in the sensitivity-limited regime are denoted $m_{s,y}$ for the youngest and $m_{s,o}$ for the oldest age.

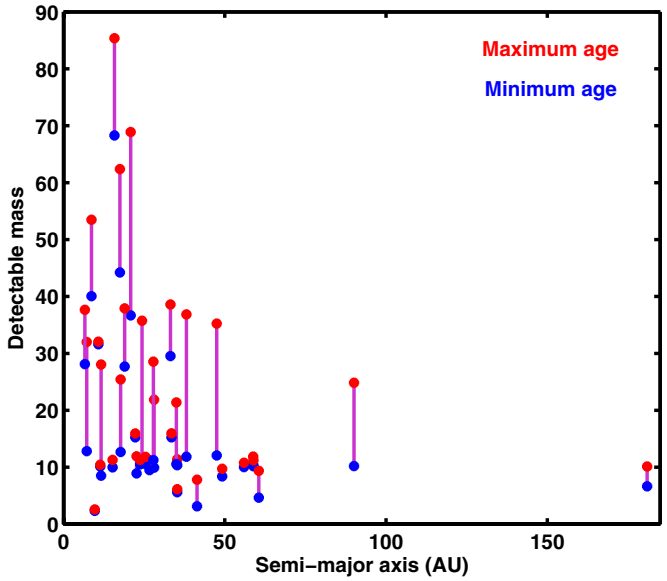

Figure 9. Detectable mass and semi-major axis at the estimated gap edge of the debris disks. The blue points are the masses at the lower age limit, and the red points are the masses at the upper limit.

(A color version of this figure is available in the online journal.)

the absence of heating from deuterium burning in the COND/DUSTY models may conversely underpredict the brightness for a given mass and age (Mollière & Mordasini 2012). Nonetheless, the uncertainties in mass–luminosity relationships is a further uncertainty that should be kept in mind.

In order to put the issue of gap-opening super-Jupiters in a statistical context, we evaluate the probability that planets with masses similar to that of β Pic b of $\sim$10 $M_{\rm jup}$ (Bonnefoy et al. 2013 and T. Currie et al. in preparation) would be detectable near the gap in each observed system. This is done by calculating the full projected separation distribution corresponding to a semi-major axis of $a_{\rm dust}$ for random orbital orientations and a uniform eccentricity distribution between 0.0 and 0.6 (Janson et al. 2011; Bonavita et al. 2012). The fraction of 10 $M_{\rm jup}$ planets that are detectable in a given system is denoted $f_{\rm y}$ for the lower limit of the age of the star and $f_{\rm o}$ for the upper limit. The individual values of $f_{\rm y}$ and $f_{\rm o}$ are listed in Table 4. In some of the systems, such a planet is simply not detectable (0% in both $f_{\rm y}$ and $f_{\rm o}$), while in the best cases the fraction is close to 100%. From the collection of these values and the fact that no planets were detected in the sample, we can estimate an upper limit on the frequency of planets with equal or higher mass than β Pic b near the estimated gap edge, using Bayes theorem following the procedure in Janson et al. (2011). As a result, we find that at 95% confidence, $<$15.2% of the stars host such planets in the extreme case where the younger age limit is adopted in all cases, and $<$30.1% in the opposite case where the upper limits are adopted. In other words, if giant planets are a dominant cause of gaps in debris disks, then the majority of them must be less massive than β Pic b. In either case, it implies that β Pic b is probably in the upper mass range of any gap-causing planets that may exist.

An illustration of typical mass detection limits around $a_{\rm dust}$ for the individual stars is shown in Figure 9, where the detectable mass is evaluated at $\alpha_{\rm dust} = a_{\rm dust}/d/1.26$, which represents the average angular separation of a planet with semi-major axis $a_{\rm dust}$ for random orbital orientations (Fischer & Marcy 1992). Here, d denotes the distance to the target. The mass limits in our survey are contrast-limited rather than sensitivity-limited, hence it would be possible to substantially enhance the limits with upcoming extreme AO-assisted instruments such as SPHERE, GPI, or CHARIS (Beuzit et al. 2008; Macintosh et al. 2008; Peters et al. 2012). These facilities may thus be able to detect a large number of gap-opening super-Jupiters if they are relatively common, or otherwise put yet more stringent limits on their presence and properties.

6. CONCLUSIONS

In this study, we have presented high-contrast imaging of a sample of 50 stars primarily in the G–A-type range with known infrared excess due to debris disks, using the HiCIAO camera at the Subaru telescope. Targets were particularly selected if they had excess only at long wavelengths, implying cold debris disks with an inner gap, possibly carved out by massive planets within the disk. The targets were observed both in order to attempt to spatially resolve the disk, as well as to try to detect the putative planets that may be responsible for the disk morphology. No planets were discovered, despite the fact that β Pic b-like planets ($\sim$10 $M_{\rm jup}$) could have been detected near the estimated gap edges in many cases. This led to an upper limit of 15%–30% on the frequency of such planets, implying that if planets are a general cause of the commonly existing gaps in debris disk systems, then they must generally be lower in mass than β Pic b. Five debris disks have been spatially resolved during the survey, two of which have already been presented in previous publications (Thalmann et al. 2011, 2013). Future studies with upcoming instrumentation will be able to put yet more stringent constraints on planet occurrences in debris disk systems, by probing down to smaller planetary masses and smaller semi-major axes, and thus may conclusively address whether the gaps in debris disks are typically caused by planets, or whether other mechanisms dominate the disk architecture.

Support for this work was provided by NASA through Hubble Fellowship grant HF-51290.01 awarded by the Space Telescope Science Institute, which is operated by the Association of Universities for Research in Astronomy, Inc., for NASA, under contract NAS 5-26555. J.C. was supported by NSF award 1009203. Archival data from the Subaru, Gemini, Keck and Hubble telescopes have been used as part of this study. We acknowledge the cultural significance of Mauna Kea to the indigenous population of Hawaii. This study made use of the CDS services SIMBAD and VizieR, as well as the SAO/NASA ADS service.

REFERENCES

Acke, B., Min, M., Dominik, C., et al. 2012, A&A, 540, 125
Allard, F., Hauschildt, P., Alexander, D., Tamanai, A., & Schweitzer, A. 2001, ApJ, 556, 357
Apai, D., Janson, M., Moro-Martín, A., et al. 2008, ApJ, 672, 1196
Ardila, D. R., Golimowski, D. A., Krist, J. E., et al. 2004, ApJL, 617, L147
Artigau, E., Biller, B. A., Wahhaj, Z., et al. 2008, Proc. SPIE, 7014, 66
Baraffe, I., Chabrier, G., Barman, T., Allard, F., & Hauschildt, P. 2003, A&A, 402, 701
Beichman, C. A., Bryden, G., Stapelfeldt, K. R., et al. 2006, ApJ, 652, 1674
Beichman, C. A., Lisse, C. M., Tanner, A. M., et al. 2011, ApJ, 743, 85
Beuzit, J. L., Feldt, M., Dohlen, K., et al. 2008, Proc. SPIE, 7014, 41
Bonavita, M., Chauvin, G., Desidera, S., et al. 2012, A&A, 537, 67
Bonnefoy, M., Boccaletti, A., Lagrange, A. M., et al. 2013, A&A, in press (arXiv:1302.1160)
Booth, M., Kennedy, G., Sibthorpe, B., et al. 2013, MNRAS, 428, 1263
Borucki, W. J., Koch, D. G., Basri, G., et al. 2011, ApJ, 736, 19
Brandt, T. D., McElwain, M. W., Turner, E. L., et al. 2013, ApJ, 764, 183

Buenzli, E., Thalmann, C., Vigan, A., et al. 2010, A&A, 524, L1
Carpenter, J. M., Bouwman, J., Mamajek, E. E., et al. 2009, ApJS, 181, 197
Carson, J., Thalmann, C., Janson, M., et al. 2013, ApJL, 763, L32
Casagrande, L., Schönrich, R., Asplund, M., et al. 2011, A&A, 530, 138
Chabrier, G., Baraffe, I., Allard, F., & Hauschildt, P. 2000, ApJ, 542, 464
Chauvin, G., Lagrange, A. M., Udry, S., et al. 2006, A&A, 456, 1165
Chen, C. H., Mamajek, E. E., Bitner, M. A., et al. 2011, ApJ, 738, 122
Chen, C. H., Sargent, B. A., Bohac, C., et al. 2006, ApJS, 166, 351
Clampin, M., Krist, J. E., Ardila, D. R., et al. 2003, AJ, 126, 385
Currie, T., Debes, J., Rodigas, T. J., et al. 2012a, ApJL, 760, L32
Currie, T., Rodigas, T. J., Debes, J., et al. 2012b, ApJ, 757, 28
Debes, J. H., Weinberger, A. J., & Song, I. 2008, ApJL, 684, L41
de Zeeuw, P. T., Hoogerwerf, R., de Bruijne, J. H. J., Brown, A. G. A., & Blaauw, A. 1999, AJ, 117, 354
Dodson-Robinson, S. E., Beichman, C. A., Carpenter, J. M., & Bryden, G. 2011, AJ, 141, 11
Ertel, S., Wolf, S., Metchev, S., et al. 2011, A&A, 533, 132
Fischer, D., & Marcy, G. 1992, ApJ, 396, 178
Galicher, R., Marois, C., Zuckerman, B., & Macintosh, B. 2013, ApJ, 769, 42
Golimowski, D. A., Krist, J. E., Stapelfeldt, K. R., et al. 2011, AJ, 142, 30
Grady, C. A., Muto, T., Hashimoto, J., et al. 2013, ApJ, 762, 48
Greaves, J. S., Holland, W. S., Wyatt, M. C., et al. 2005, ApJL, 619, L187
Hayano, Y., Takami, H., Guyon, O., et al. 2008, Proc. SPIE, 7015, 25
Heinze, A. N., Hinz, P. M., Kenworthy, M., Miller, D., & Sivanandam, S. 2008, ApJ, 688, 583
Heinze, A. N., Hinz, P. M., Sivanandam, S., et al. 2010, ApJ, 714, 1551
Hillenbrand, L. A., Carpenter, J. M., Kim, J. S., et al. 2008, ApJ, 677, 630
Hines, D., Schneider, G., Hollenbach, D., et al. 2007, ApJL, 671, L165
Hodapp, K. W., Jensen, J. B., Irwin, E. M., et al. 2003, PASP, 115, 1388
Hodapp, K. W., Suzuki, R., Tamura, M., et al. 2008, Proc. SPIE, 7014, 42
Jalali, M. A., & Tremaine, S. 2012, MNRAS, 421, 2368
Janson, M., Bonavita, M., Klahr, H., et al. 2011, ApJ, 736, 89
Janson, M., Brandner, W., Lenzen, R., et al. 2007, A&A, 462, 615
Janson, M., Carson, J., Lafrenière, D., et al. 2012, ApJ, 747, 116
Janson, M., Reffert, S., Brandner, W., et al. 2008, A&A, 488, 771
Kalas, P., Duchene, G., Fitzgerald, M. P., & Graham, J. R. 2007a, ApJL, 671, L161
Kalas, P., Fitzgerald, M. P., & Graham, J. R. 2007b, ApJL, 661, L85
Kalas, P., Graham, J., & Clampin, M. 2005, Natur, 435, 1067
Kalas, P., Graham, J. R., Chiang, E., et al. 2008, Sci, 322, 1345
Kalas, P., Graham, J. R., Clampin, M. C., & Fitzgerald, M. P. 2006, ApJL, 637, L57
Kasper, M., Apai, D., Janson, M., & Brandner, W. 2007, A&A, 472, 321
Kenworthy, M. A., Meshkat, T., Quanz, S. P., et al. 2013, ApJ, 764, 7
Kobayashi, N., Tokunaga, A. T., Terada, H., et al. 2000, Proc. SPIE, 4008, 1056
Köhler, R., & Leinert, C. 1998, A&A, 331, 977
Krist, J. E., Ardila, D. R., Golimowski, D. A., et al. 2005, AJ, 129, 1008
Krist, J. E., Stapelfeldt, K. R., Bryden, G., et al. 2010, AJ, 140, 1051
Kusakabe, N., Grady, C. A., Sitko, M. L., et al. 2012, ApJ, 753, 153
Lafrenière, D., Doyon, R., Marois, C., et al. 2007a, ApJ, 670, 1367
Lafrenière, D., Marois, C., Doyon, R., Nadeau, D., & Artigau, E. 2007b, ApJ, 660, 770
Lagrange, A.-M., Bonnefoy, M., Chauvin, G., et al. 2010, Sci, 329, 57
Lagrange, A.-M., Gratadour, D., Chauvin, G., et al. 2009, A&A, 493, L21
Lawler, A. M., Beichman, C. A., Bryden, G., et al. 2009, ApJ, 705, 89
López-Santiago, J., Montes, D., Crespo-Chacón, I., & Fernández-Figueroa, M. J. 2006, ApJ, 643, 1160
Lovis, C., Mayor, M., Pepe, F., et al. 2006, Natur, 441, 305
Lyra, W., & Kuchner, M. J. 2012, ApJ, submitted (arXiv:1204.6322)
Macintosh, B., Graham, J. R., Palmer, D. W., et al. 2008, Proc. SPIE, 7015, 31
Maldonado, J., Martínez-Arnáiz, R. M., Eiroa, C., Montes, D., & Montesinos, B. 2010, A&A, 521, 12
Mamajek, E. E., & Hillenbrand, L. A. 2008, ApJ, 687, 1264
Marleau, G.-D., & Cumming, A. 2013, MNRAS, submitted (arXiv:1302.1517)
Marois, C., Lafrenière, D., Doyon, R., Macintosh, B., & Nadeau, D. 2006, ApJ, 641, 556
Marois, C., Macintosh, B., Barman, T., et al. 2008, Sci, 322, 1348
Marois, C., Zuckerman, B., Konopacky, Q., Macintosh, B., & Barman, T. 2010, Natur, 468, 1080
Mason, B. D., Wycoff, G. L., Hartkopf, W. I., Douglass, G. G., & Worley, C. E. 2001, AJ, 122, 3466
Mayor, M., & Queloz, D. 1995, Natur, 378, 355
McLean, I. S., & Sprayberry, D. 2003, Proc. SPIE, 4841, 1
Merín, B., Montesinos, B., Eiroa, C., et al. 2004, A&A, 419, 301
Metchev, S. A., & Hillenbrand, L. A. 2009, ApJS, 181, 62
Meyer, M. R., Carpenter, J. M., Mamajek, E. E., et al. 2008, ApJL, 673, L181
Mollière, P., & Mordasini, C. 2012, A&A, 547, 105
Moór, A., Apai, D., Pascucci, I., et al. 2009, ApJL, 700, L25
Moór, A., Pascucci, I., Kóspál, Á., et al. 2011, ApJS, 193, 4
Morales, F. Y. 2009, ApJ, 699, 1067
Muto, T., Grady, C. A., Hashimoto, J., et al. 2012, ApJL, 748, L22
Pecaut, M. J., Mamajek, E. E., & Bubar, E. J. 2012, ApJ, 746, 154
Peters, M. A., Groff, T., Kasdin, N. J., et al. 2012, Proc. SPIE, 8446, 7
Plavchan, P., Werner, M. W., Chen, C. H., et al. 2009, ApJ, 698, 1068
Quanz, S., Amara, A., Meyer, M. R., et al. 2013, ApJL, 766, L1
Quillen, A. C. 2006, MNRAS, 372, L14
Quillen, A. C., & Thorndike, S. 2002, ApJL, 578, L149
Rameau, J., Chauvin, G., Lagrange, A.-M., et al. 2013, A&A, 553, 60
Rhee, J. H., Song, I., Zuckerman, B., & McElwain, M. 2007, ApJ, 660, 1556
Rieke, G. H., Su, K. Y. L., Stansberry, J. A., et al. 2005, ApJ, 620, 1010
Rodigas, T. J., Hinz, P. M., Leisenring, J., et al. 2012, ApJ, 752, 57
Saffe, C., Gómez, M., & Chavero, C. 2005, A&A, 443, 609
Santos, N., Israelian, G., Mayor, M., Rebolo, R., & Udry, S. 2003, A&A, 398, 363
Schneider, G., Smith, B. A., Becklin, E. E., et al. 1999, ApJL, 513, L127
Schneider, G., Weinberger, A. J., Becklin, E. E., Debes, J. H., & Smith, B. A. 2009, AJ, 137, 53
Schultz, A. B., Sosey, M., Mazzuca, L. M., et al. 2003, Proc. SPIE, 4850, 858
Setiawan, J., Weise, P., Henning, T., et al. 2007, ApJL, 660, L145
Smith, B. A., & Terrile, R. J. 1984, Sci, 226, 1421
Smith, R., Wyatt, M. C., & Haniff, C. A. 2009, A&A, 503, 265
Song, I., Zuckerman, B., & Bessell, M. S. 2012, AJ, 144, 8
Spiegel, D. S., & Burrows, A. 2012, ApJ, 745, 174
Su, K. Y. L., Rieke, G. H., Stansberry, J. A., et al. 2006, ApJ, 653, 675
Tamura, M. 2009, in AIP Conf. Ser. 1158, Exoplanets and Disks: Their Formation and Diversity, ed. T. Usuda, M. Tamura, & M. Ishii (Melville, NY: AIP), 11
Tamura, M., Hodapp, K., Takami, H., et al. 2006, Proc. SPIE, 6269, 62690V
Thalmann, C., Janson, M., Buenzli, E., et al. 2011, ApJL, 743, L6
Thalmann, C., Janson, M., Buenzli, E., et al. 2013, ApJL, 763, L29
Trilling, D. E., Bryden, G., Beichman, C. A., et al. 2008, ApJ, 674, 1086
van Leeuwen, F. 2007, A&A, 474, 653
Vican, L. 2012, AJ, 143, 135
Weinberger, A. J., Rich, R. M., Becklin, E. E., Zuckerman, B., & Matthews, K. 2000, ApJ, 544, 937
Wilner, D. J., Andrews, S. M., & Hughes, A. M. 2011, ApJL, 727, L42
Zuckerman, B., & Song, I. 2004, ARA&A, 42, 685
Zuckerman, B., & Song, I. 2012, ApJ, 758, 77